FINGERPRINTING OF TWO DIAMONDS CUT FROM THE SAME ROUGH

By Ichiro Sunagawa, Toshikazu Yasuda, and Hideaki Fukushima

If it can be determined that two faceted diamonds came from the same piece of rough, romantic value is added to the stones. X-ray topography and cathodoluminescence (CL) tomography were used to prove that a round brilliant and a pear-shaped brilliant were cut from the same piece of rough. With these techniques, the internal imperfections and inhomogeneities that reflect the distinctive growth history of the original diamond crystal can be seen. X-ray topography is a powerful tool for imaging the distribution of lattice defects; CL tomography is more sensitive for detecting faint chemical inhomogeneities. By combining the two methods, the sophisticated gemologist can view both physical and chemical characteristics of a crystal, and thus its growth history, and use this information to fingerprint a given stone.

ABOUT THE AUTHORS

Dr. Sunagawa is principal of the Yamanashi Institute of Gemmology and Jewellery Arts in Kofu, Japan, and professor emeritus of mineralogy at Tohoku University, Sendai, Japan. Mr. Yasuda recently retired from the Geological Survey of Japan in Tsukuba, Ibaraki Prefecture, where he was a specialist in the X-ray topography of crystals. Mr. Fukushima is a member of the Education Department at the Gemmological Association of All Japan in Tokyo, where he has taken thousands of cathodoluminescence tomographs of faceted diamonds.

The authors express their thanks to Mr. M. Ishida of ExRoyal Inc., New York, for providing the samples.

Gems & Gemology, *Vol. 34, No. 4, pp. 270–280*

Typically, two faceted stones are cut from one well-formed diamond crystal. Yet each takes a different route in the market, with little chance of both diamonds being set together in a single piece or related pieces of jewelry. However, if two such diamonds were set in two pieces of jewelry worn, for example, by a mother and a daughter, this might provide additional sentimental value to the stones. Keeping two such diamonds together is possible only when the piece of rough is cut under the dealer's control. Even so, scientific documentation is necessary to prove this shared origin. Plotting a diamond's internal features (as in a diamond grading report) may help identify a single stone, but it cannot prove that two diamonds came from the same rough. More advanced techniques are needed for this task.

Natural crystals do not grow at a constant rate or under constant conditions. Rather, crystals may experience growth-rate fluctuations, gentle or abrupt changes in growth parameters, or partial dissolution and regrowth during their formation. As a result, physical imperfections and chemical inhomogeneities—such as inclusions, lattice defects (point defects, dislocations, and planar defects), and chemical impurities—are induced in crystals during their growth and postgrowth histories. These characteristics are uniquely distributed within each crystal as growth sectors (zonal structures), intrasectorial zoning, growth banding, and nonuniform distributions of elements, color, or luminescence; these features are not modified during later cutting and polishing processes (Sunagawa, 1984a, 1988; Scandale, 1996; and the references therein). Consequently, they are the most reliable diagnostic features for fingerprinting stones (and for distinguishing natural from synthetic gem minerals; see, e.g., Sunagawa, 1995), provided they can be determined nondestructively.

We report in this article how we verified that two diamonds—a round brilliant and a pear-shaped brilliant—came from the same piece of rough, by revealing the spatial distri-

Figure 1. These three diamonds, all from the same manufacturer, were studied to determine which two, if any, were cut from the same piece of rough. All of the diamonds were graded as E color and VS_1 clarity. Sample A (left) weighs 1.08 ct, sample B (center) is 0.81 ct, and sample C (right) weighs 1.05 ct. Samples B and C were proved to originate from the same rough diamond.

bution of lattice defects (using X-ray topography) and those of cathodoluminescence-emitting centers (using CL tomography). Both methods were applied without any damage to the stones.

The study was initiated when a dealer claimed that two brilliant-cut diamonds he was offering were from the same rough. After X-ray topography proved otherwise, the dealer traced the route the two stones had taken from the cutter, and eventually he found another brilliant that produced an X-ray topograph that matched one of the previous brilliants. After establishing the characteristics of these three diamonds by X-ray topography, the authors applied CL tomography to provide supporting evidence for the initial conclusions. The characteristics observed with these two techniques vividly demonstrate the different growth histories of different diamond crystals. This example also demonstrates the usefulness and applicability of X-ray topography and CL tomography in gemology.

MATERIALS AND METHODS

Samples. The first pair of diamonds offered by the dealer, samples A and B, had the following characteristics recorded on their GIA Gem Trade Laboratory (GIA GTL) grading reports:

> **Sample A:** Round brilliant; 1.08 ct; 6.59–6.62 × 4.10 mm; E color; VS_1 clarity; 62.1% depth, 56% table, thin-to-medium faceted girdle, no culet; excellent polish; very good symmetry; no fluorescence (report dated February 9, 1993).

> **Sample B:** Pear-shaped brilliant; 0.81 ct; 8.03 × 5.54 × 2.93 mm; E color; VS_1 clarity; 52.9% depth, 55% table, thin-to-thick faceted girdle, very small culet; good polish; good symmetry; no fluorescence (report dated January 4, 1993).

As described below, it was proved that these two diamonds were not cut from the same piece of rough. Subsequently, the dealer traced the stones back to the manufacturer and submitted the following diamond, sample C:

> **Sample C:** Round brilliant; 1.05 ct; 6.43–6.67 × 4.01 mm; E color; VS_1 clarity; 60.3% depth, 59% table, very thin-to-thin faceted girdle, small culet; excellent polish; very good symmetry; no fluorescence (report dated January 25, 1993).

Samples A, B, and C are shown in figure 1. They are very clean to the naked eye and, as evident from the GIA GTL grading reports, no internal flaws are discernible with the microscope, other than pinpoint inclusions. Nevertheless, X-ray topography and CL tomography (as described below) revealed distinctive internal heterogeneities and imperfections.

Experimental Procedures. *X-Ray Topography.* By identifying contrasts in X-ray reflection, X-ray topography can detect and record the spatial distribution of strain fields associated with various linear defects (e.g., dislocations) and planar defects (e.g., stacking faults and twin planes) in single crystals. In other words, X-ray topography reveals the distribution of deviations from the ideal lattice plane. The term *topography* is used to describe the three-dimensional nature of these data.

Since X-ray topography is a well-established

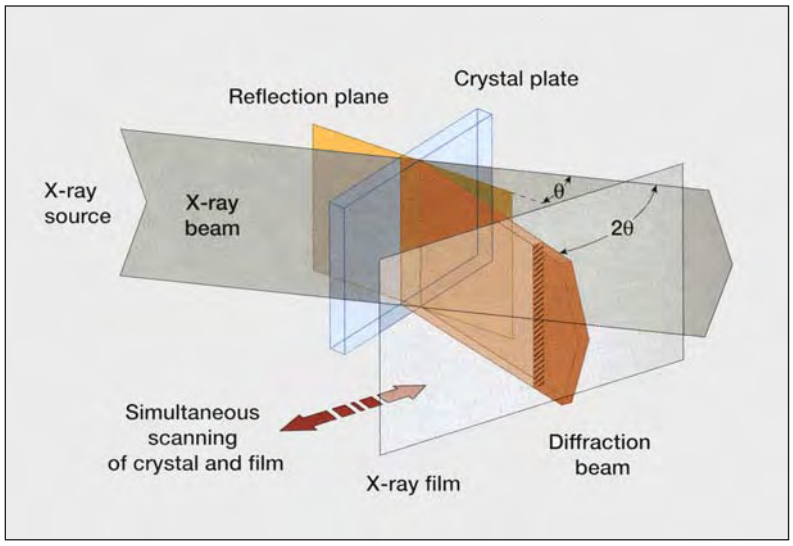

Figure 2. This schematic diagram illustrates the geometry generally adopted to obtain X-ray topographs (after Lang, 1978). In the present study, a faceted diamond was used in place of the crystal plate, with the table facet parallel or perpendicular to the plate (see figure 3). X-rays are passed through a narrow slit and reflected through the sample, off one selected lattice reflection plane, to produce a three-dimensional image of the crystallographic imperfections and inhomogeneities on the X-ray film. The three-dimensional image is obtained by scanning the entire sample, through synchronous movement of both sample and film.

method, this article will not give a detailed description of its principles and methods. Interested readers may refer to review papers by Frank and Lang (1965) or Lang (1978, 1979).

In the present study, the Lang method (1978) was used to record the X-ray topographs (see figure 2). The sample is typically cut into a plate for analysis, but complete crystals or faceted stones can be used if the sample is small; good topographs can be obtained for diamonds up to about 2 ct. A narrow, ribbon-like beam of X-rays with a fixed wavelength is passed through a narrow slit and scanned over the sample at a fixed incident angle (i.e., in a reflection orientation). Only those X-ray beams that match the ideal reflection of the lattice plane are reflected off this plane and recorded on the X-ray film. Distorted lattice portions (i.e., those that deviate from the ideal reflection plane) appear as contrasting images on the film (white on the negative, or black on the print), thus revealing the spatial distribution of lattice defects in the sample. The X-rays used in this study were produced with an accelerat-

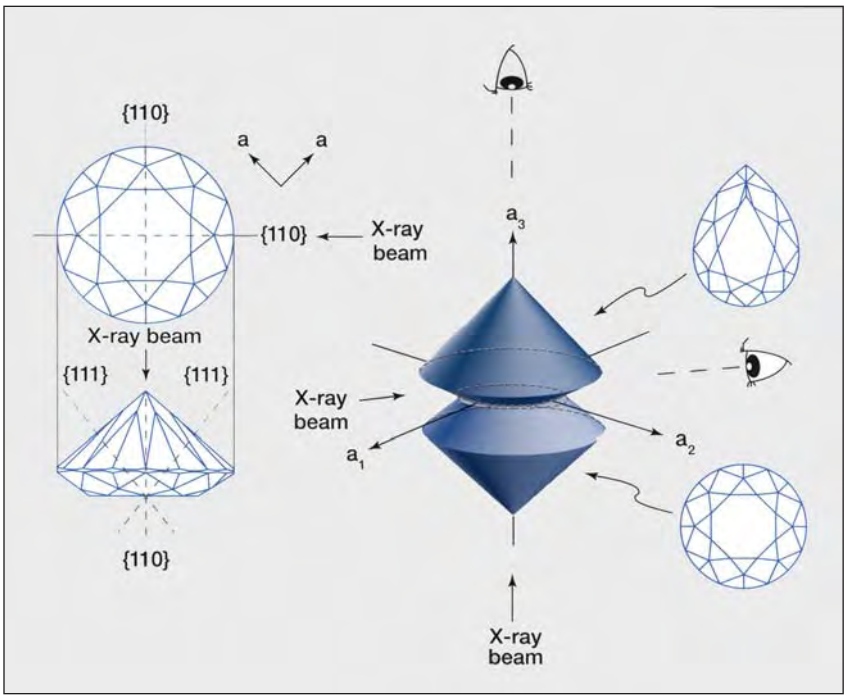

Figure 3. For this study, {110} and {111} crystallographic planes (dashed lines) were selected as the lattice reflection planes (left). The orientation of two of the a-axes are shown. Two directions of the incident X-ray beams were used in this study—parallel and perpendicular to the table facet (horizontal and vertical, respectively). The schematic diagram on the right shows the viewing geometry for the samples. The round brilliant indicates the positions of samples A and C, and the pear-shaped brilliant indicates sample B. The two directions of view in the corresponding X-ray topographs are indicated by the eyes. Note that the reflection plane {220} is expressed as {110} for simplicity in this article; {110} does not reflect X-ray beams, but {220} does.

ing voltage of 50 kV and a current of 1 mA.

For X-ray topography, the system operator must select appropriate lattice reflection planes, taking into consideration the angles and intensities of reflecting beams and the distortion of images caused by the oblique scanning angle. Assuming that the table facet in each stone was approximately parallel to a (100) plane, we selected {110} and {111} directions as reflection planes. (Note that the reflection plane {220} is expressed as {110} for simplicity in this article; according to the extinction rule, {110} does not reflect X-ray beams, but {220} does.) This is shown schematically in figure 3. As figure 4 illustrates, the images are distorted depending on the direction of the reflection. This distortion must be taken into consideration when the X-ray topographs for two different stones are compared. To obtain images with good contrast, the researcher usually prepares a plate from the sample that is of appropriate thickness (depending on the material, e.g., 1 mm for quartz). This, of course, is not possible with polished gemstones. However, because good topographs can be achieved with relatively thick samples of diamond, we were able to obtain useful images from the faceted stones examined for this study.

Cathodoluminescence Tomography. After we had analyzed all three samples by X-ray topography, we used CL tomography as a supporting method. With this technique, one can see the heterogeneous distribution of CL-emitting centers in a solid material, up to a few micrometers below the surface. Because of the limited depth of penetration, this technique is referred to as *tomography*, since it reveals only the two-dimensional distribution of the CL-emitting centers in a plane near the surface. CL tomography has been used widely in solid-state physics and the earth sciences (see, e.g., Davies, 1979; Lang, 1979), and Ponahlo (1992) has also applied it to gemology.

A scanning electron microscope (SEM) or optical microscope is used to observe the images generated by CL tomography. The present study used the latter, a Premier American Technologies Co. Luminoscope. Because of its lower vacuum, the Luminoscope is not as sensitive as an SEM system, but it is adequate for this type of problem. Also, the samples do not need to be carbon-coated (as they would for SEM analysis). CL tomography does not automatically identify the elements responsible for the CL emission; nor does it give quantitative data for their concentrations. The CL intensities may correspond semi-quantitatively to the concentrations of the CL-emitting centers, but other methods, such as spectroscopy, are required to identify the chemical elements or obtain quantitative data. However, for the purpose of this study—that is, visualizing the distribution of CL-emitting centers in different diamonds—quantitative analyses were not needed.

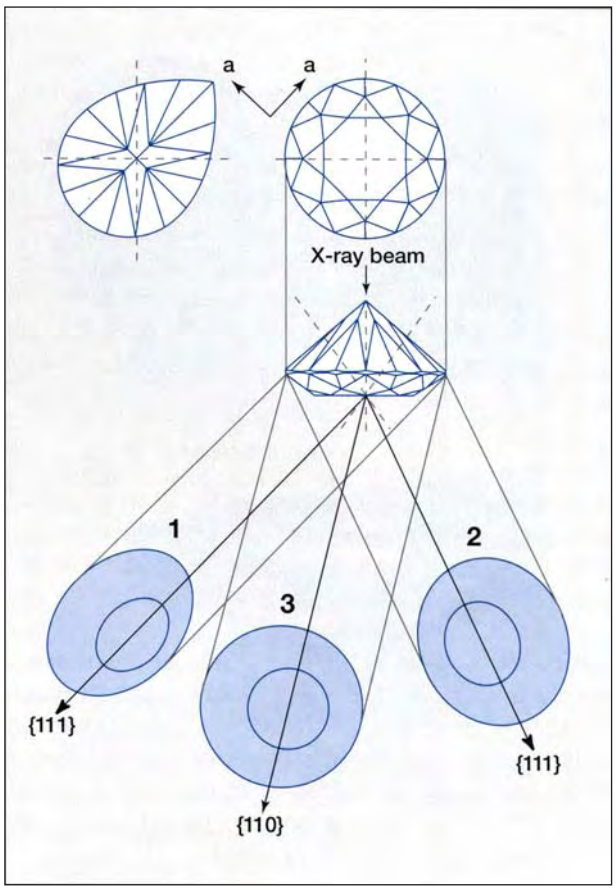

Figure 4. X-ray topographic images are distorted because of the oblique reflection of the vertical X-ray beam. Here, three schematic diagrams—each labeled with the corresponding reflection plane—{110} or {111}—illustrate the positions of the table facet (small circles) and the girdle outline; the profile of each stone is also shown. All three images are produced using the same (vertical) incident X-ray direction; the particular image obtained depends on the reflection plane selected. Note that the image in 2 is inverted relative to 1. Actual X-ray topographs corresponding to these three images are shown in figure 5.

RESULTS

X-Ray Topography. *Samples A and B.* X-ray topographs of sample A, taken with {110} and {111}

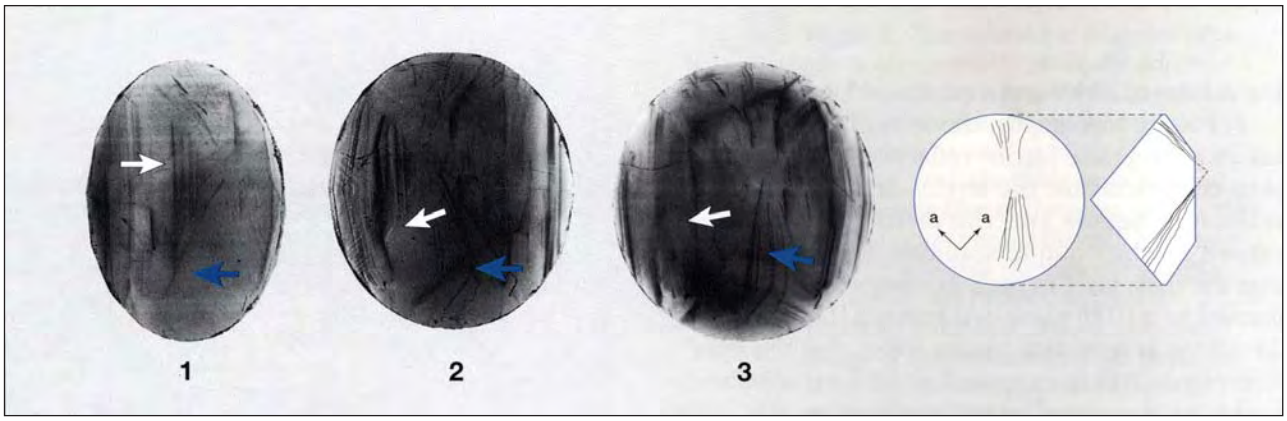

Figure 5. These three X-ray topographs of sample A were taken with different reflection planes, as shown in figure 4 (images 1, 2, and 3). The green arrows indicate dislocations, and the white arrows indicate growth banding. An idealized illustration of the dislocations is shown for topograph 3, in plan view and in profile. The two dislocation bundles are inferred to meet at a position slightly above the table facet.

lattice reflections, show a few dislocations that are nearly parallel to {110}, and straight growth bands parallel to {111}, planes (figure 5). The dislocations radiate from a point slightly above the table facet; this point marks the center of an octahedral crystal, from which the dislocations progressed nearly perpendicular to the growing octahedral {111} faces.

X-ray topographs of sample B (figure 6) are markedly different from those of sample A. The sample B topographs reveal dislocation bundles that are much greater in number and density than those in sample A. Moreover, the dislocations in sample B are parallel to <100>, not to {110} as in sample A. The dislocation bundles originate not from a point center, but from the boundary of a square-shaped core. Faint growth banding is discernible in areas between the dislocation bundles, but these are more evident on CL tomographs (see below). The growth

Figure 6. These two X-ray topographs of sample B were taken with two (110) reflection planes. A large number of dislocations (dark heavy lines) originate from the boundaries of a square-shaped core, and form bundles nearly parallel to the a-axes. Faint zigzag patterns are also visible between the dislocations. Note the marked difference of these topographs from those of sample A shown in figure 5, with respect to the presence of a core portion, the number and orientation of dislocations, and the modes of growth banding.

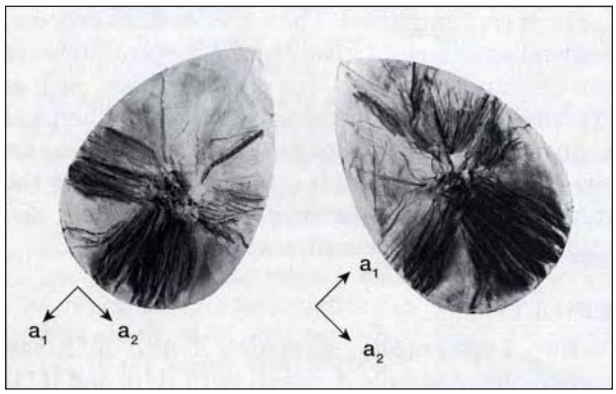

Figure 7. These X-ray topographs of sample C correspond to the same orientation and reflection planes as those shown in figure 6 for sample B. Note the close similarity to sample B in the presence of a square-shaped core portion, the density and orientation of dislocation bundles, and the faint zigzag patterns between the dislocations. The close resemblance shown by these topographs (considering that both diamonds had some material polished away) indicates that samples B and C came from the same rough.

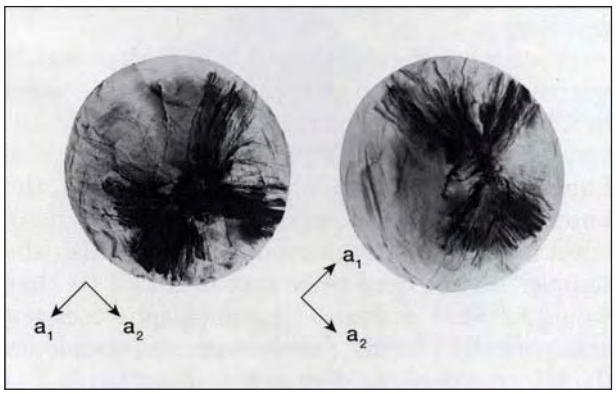

banding is not straight, but rather shows a zigzag pattern. The differences in the X-ray topographs of samples A and B suggest that they could not have originated from the same piece of rough.

Sample C. X-ray topographs of sample C (figure 7) show dislocation bundles originating from the boundary of a square-shaped core and running parallel to <100>, as well as faint zigzag patterns in the areas between the dislocation bundles. By comparing the topographs of samples B and C, one can see that the presence of the square-shaped core, the orientation and spatial distribution of the dislocations, and the faint zigzag growth banding seen in these diamonds, are essentially the same. This implies that these two diamonds were cut from the same piece of rough.

Closer observation of the core portions of samples B and C confirms their similarity (figure 8). In both samples, the dislocation densities are much higher in the surrounding portion than in the core. Although most of the dislocations in the core continue into the surrounding portion of the diamond, it is clear that most of the dislocations outside the core are generated along the boundary between the core and the surrounding diamond. It is also evident that the core portion was bounded by somewhat rugged cuboid faces. The characteristics and sizes of the core portions of samples B and C match perfectly, if the volume of the portion that was polished away from both samples is taken into consideration.

In profile view, X-ray topographs of samples B and C at the same orientation also show good correlation in the morphology and position of the core and the spatial distribution of dislocation bundles (figure 9). In addition, one notices that the table facets of the two stones are inclined slightly (about 6°–7°) from the (100) face. This inclination may be due to the cutter's desire to avoid inclusions that were originally present in the rough, or simply to obtain a higher yield from odd-shaped rough.

The results of our X-ray topographic investigations are summarized in figure 10. The images conclusively indicate that samples B and C came from the same diamond rough, whereas sample A came from a different piece of rough.

CL Tomographs. By comparing CL tomographs of samples A, B, and C (figure 11) with their X-ray topographs, one immediately notices the following:

1. Only blue cathodoluminescence of varying intensities was observed; no yellow, green, or red.

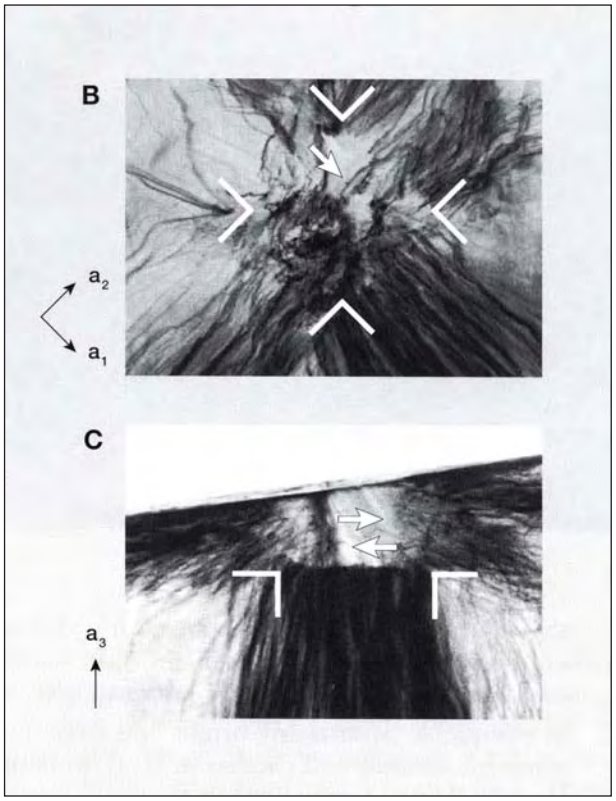

Figure 8. These X-ray topographs have been enlarged to show the core portions of samples B and C. Sample B is shown in plan view (X-ray beam perpendicular to the table facet), and sample C is shown in profile view (X-ray beam parallel to the table facet), as in figure 9. The truncation of sample C near the top of the topograph corresponds to the surface of the table facet, which shows a slight inclination relative to the (100) face. The white lines indicate the corners of the boundary of the square-shaped core, and the white arrows indicate dislocations that begin in the core and continue into the surrounding diamond. Enlarged approximately 30×.

2. Straight (sample A) or zigzag (samples B and C) growth banding, which was faintly visible on the X-ray topographs, was more readily seen on the CL tomographs (as alternating bright and dark bands).
3. The square-shaped core present on the CL tomographs of samples B (at the center of the table facet) and C (at the upper left of the table facet) is not visible in sample A, on either the X-ray topographs or the CL tomographs.
4. Although growth banding typically is easier to see on CL tomographs than on X-ray topographs,

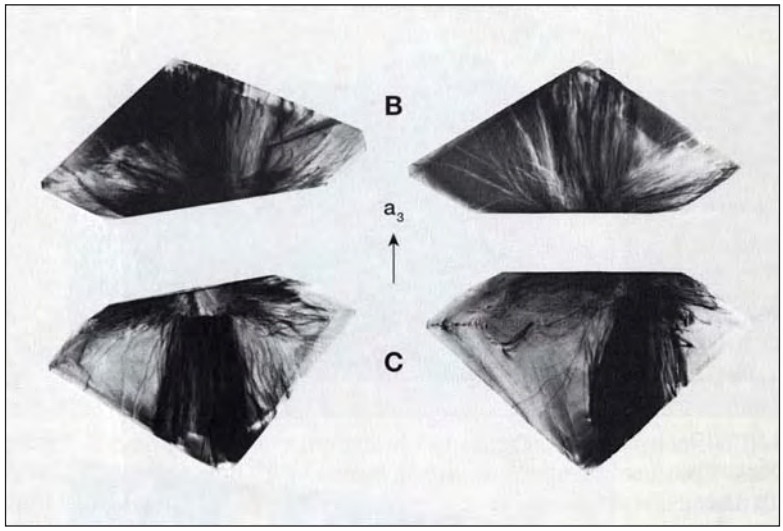

Figure 9. These X-ray topographs show two profile views of sample B (top) and sample C (bottom). The topographs are oriented to show the faceted diamonds as they were positioned in the original crystal, with the a3 axis indicated by the arrow in the center. The topographs on the right show the samples rotated 90° from those on the left; the crystallographic orientation between the upper and lower views is identical. There is a high degree of correlation between the two diamonds in the character and orientation of the dislocations. The core portion is difficult to see in sample B, because most of it has been polished away. Note also that the table facet is inclined about 6°–7° from the crystallographic (100) plane.

the radiating dislocations that are clearly visible on the X-ray topographs of samples A, B, and C could not be resolved on their CL tomographs.

5. In sample A, alternating bright and dark CL zones are straight and parallel to {111}. In both samples B and C, two different types of growth zoning can be distinguished on the CL tomographs. One type is visible between neighboring areas of the second set as short, fairly straight, bright and dark CL zones parallel to <110>. In the second set, bright and dark zones with a zigzag pattern are present within the <100> zones, which correspond to the location of dislocation bundles seen on the X-ray topographs. (Note: Since {100} faces are never present as smooth, flat faces on natural diamond crystals [Sunagawa, 1984b], they are customarily called "cuboid" faces. For simplicity, we refer to them here as <100> zones instead.)

At higher magnification, CL images of the core portions of samples B and C revealed these additional features (figure 12):

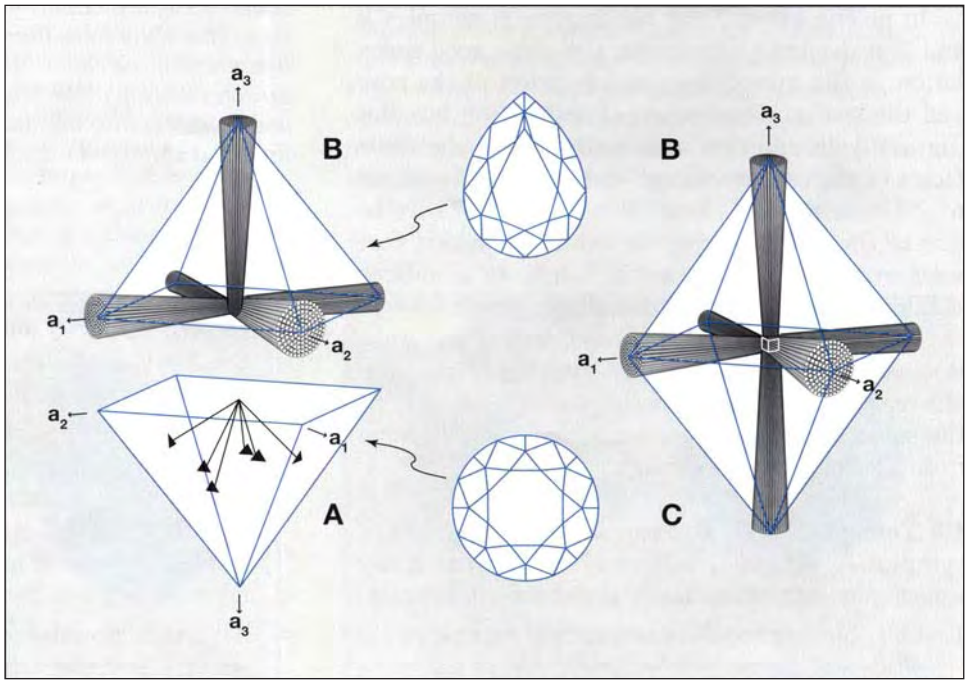

Figure 10. These diagrams schematically illustrate the three-dimensional nature of the dislocations revealed by X-ray topography in the three samples. On the left, the appearance and orientation of the dislocations in sample A (bottom) are much different from those in sample B (top). On the right, a perfect match is evident for samples B and C in the presence of a cuboid-shaped core and the analogous dislocation bundles.

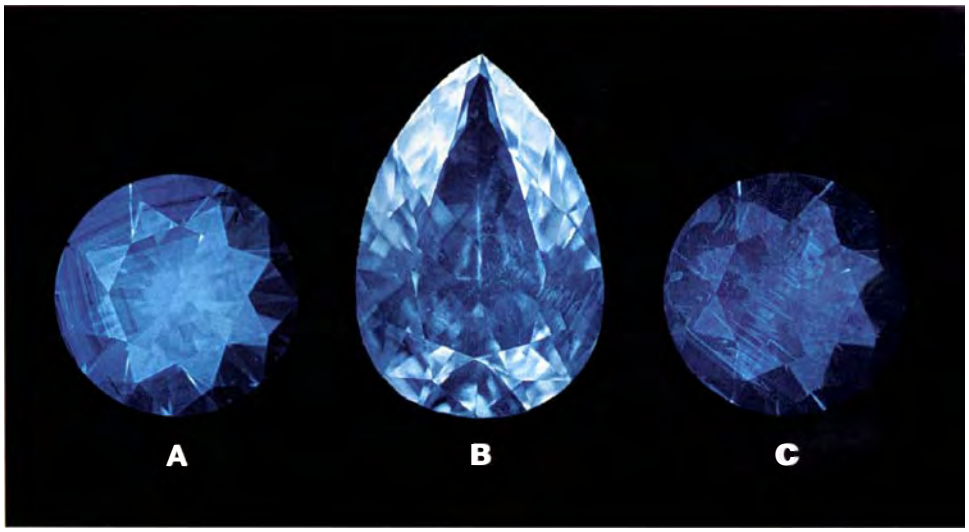

Figure 11. The distribution of CL-emitting centers is visible on these CL tomographs. Note the marked difference between sample A (e.g., straight growth zones, absence of a square-shaped core) and samples B and C (e.g., zigzag growth zones and the presence of a square-shaped core—in the center of the table of sample B and in the upper left of the table in sample C).

6. The distribution of bright and dark areas is less heterogeneous in the core portion than in the surrounding areas.
7. Around the perimeter of the core is a bright cathodoluminescence zone, which indicates a high concentration of CL-emitting centers at this boundary.
8. In the <100> growth sectors, where bundles of dislocations are visible on the X-ray topograph, bright and dark zones in the shape of a zigzag—or short right angles—appear alternately or intermittently. The segments are parallel to <110> (i.e., they consist of segmental {111} planes).
9. In the <110> growth sectors (i.e., in the areas between the neighboring <100> growth sectors), short or long bright CL bands appear parallel to <110>. These bands do not show a zigzag pattern, but rather they have a tabular form. These features correlate to a high concentration of CL-emitting species. The intervening dark bands correlate to zones that lack CL-emitting centers.
10. Both the straight bands and the zigzag segments are parallel to <110> (i.e., to {111} planes). Each straight band or segment corresponds to a small internal {111} face. Since they appear as bright CL bands, the {111} faces are apparently associated with incorporation of CL-emitting species.

Figure 12. At greater magnification (approximately 25×), the CL tomographs of samples B and C show the dark, roughly square-shaped core and surrounding brighter CL-emitting areas. Crystallographic directions <100> and <110> are indicated. Note the bright and dark zigzag patterns in the <100> sectors and the tabular patterns in the <110> sectors.

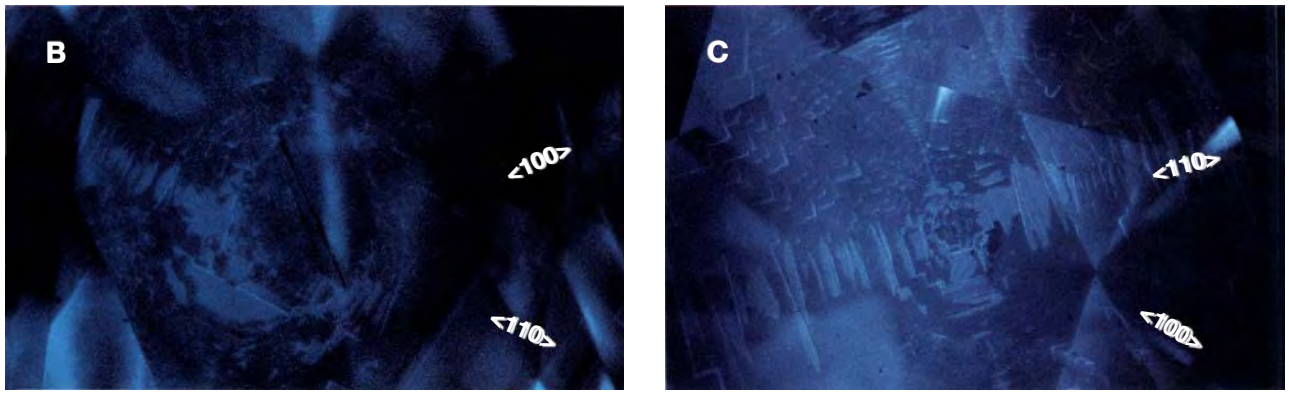

DISCUSSION

Fingerprinting Faceted Diamonds. Several features observed with X-ray topography and CL tomography prove that samples B and C were cut from the same piece of diamond rough, whereas sample A came from a different crystal. In general, the spatial distribution and orientation of dislocations, the presence or absence of a square-shaped core, and the characteristics of growth banding were distinctive for these samples.

Although the present case is unambiguous, it might be asked whether such fingerprinting is universally applicable. The answer is "yes," since each natural single crystal experienced its own unique growth or post-growth history, which is recorded in its internal imperfections and inhomogeneities. With careful investigation, one can conclusively fingerprint a stone or a set of stones, even if two stones show quite similar internal features.

Applying X-Ray Topography and CL Tomography in Gemology. Crystallographic imperfections and inhomogeneities are distinctive features that can be visualized using instruments available in many standard gemological laboratories (such as the horizontal microscope with immersion; see, e.g., Schmetzer 1996; Smith, 1996). However, X-ray topography allows the visualization of three-dimensional lattice imperfections—such as dislocations—that are not easy to visualize by other methods. CL tomography shows near-surface chemical inhomogeneities two-dimensionally. Both methods can be used to distinguish natural from synthetic diamonds (as well as any other gemstone), since in each case the crystals grow from different media and under different conditions (Lang et al., 1992; Sunagawa, 1995, 1998).

In general, X-ray topography is more informative than CL tomography. Although most major gemological laboratories have the capitalization to install a Lang configuration for X-ray topography (which can cost from $50,000 to about $100,000), the technique requires a thorough knowledge of crystallography and diffraction, and it is somewhat time consuming to adjust the crystallographic orientation of a sample to obtain good topographs.

CL tomography, in combination with optical microscopy, is also affordable (about $25,000) for most major gemological laboratories, and it does not require much background knowledge. Although it cannot reveal the spatial distribution of dislocations as effectively as X-ray topography, it is useful in fingerprinting a stone or a set of stones. Furthermore, CL data can, independent of X-ray topography, conclusively separate natural from synthetic diamonds (Ponahlo, 1992; Sunagawa, 1995).

Growth History. These techniques also provide useful information about the formation of natural diamond crystals. Arguments over the origin of natural diamonds began long ago (e.g., Fersman and Goldschmidt, 1911), and still continue (Frank and Lang, 1965; Lang, 1978, 1979; Lang et al., 1992; Sunagawa, 1984b, 1988, 1995; Sunagawa et al., 1984).

Although we did not identify the CL-emitting species in this study, or determine their concentrations, it is commonly known that blue cathodoluminescence is principally due to nitrogen (probably a combination of band-A and N3 centers) and that CL intensities correspond semi-quantitatively to nitrogen contents (Clark et al., 1992). Higher concentrations of nitrogen are assumed for the zones showing brighter CL images than for the darker zones. The CL observations in the present study indicate that nitrogen incorporation into the growing diamond crystal fluctuated intermittently, with the boundaries between the CL zones representing the positions of growing surfaces at various stages. Such fluctuations are universally observed in natural crystals.

Two distinctly different growth histories were identified for the diamonds in the present study (figure 13). In sample A, alternating bright and dark CL zones form a straight pattern parallel to {111} throughout the stone, which indicates that a simple, unmodified octahedral crystal habit was maintained throughout its entire growth history. Dislocations originate from a central point and are oriented perpendicular to {111}. These indicate that the crystal did not experience an abrupt change in growth parameters to modify the habit. Such a situation corresponds to the growth of crystals under a near-equilibrium condition at a small driving force (low supersaturation or low degrees of supercooling). Dislocation patterns of this type are commonly encountered in octahedral crystals of natural diamond (see, e.g., Frank and Lang, 1965; Lang, 1978). They have been identified as screw-type dislocations in single-crystal octahedral diamonds from Siberia (Sunagawa et al., 1984), which proves that the natural diamond crystals investigated grew by

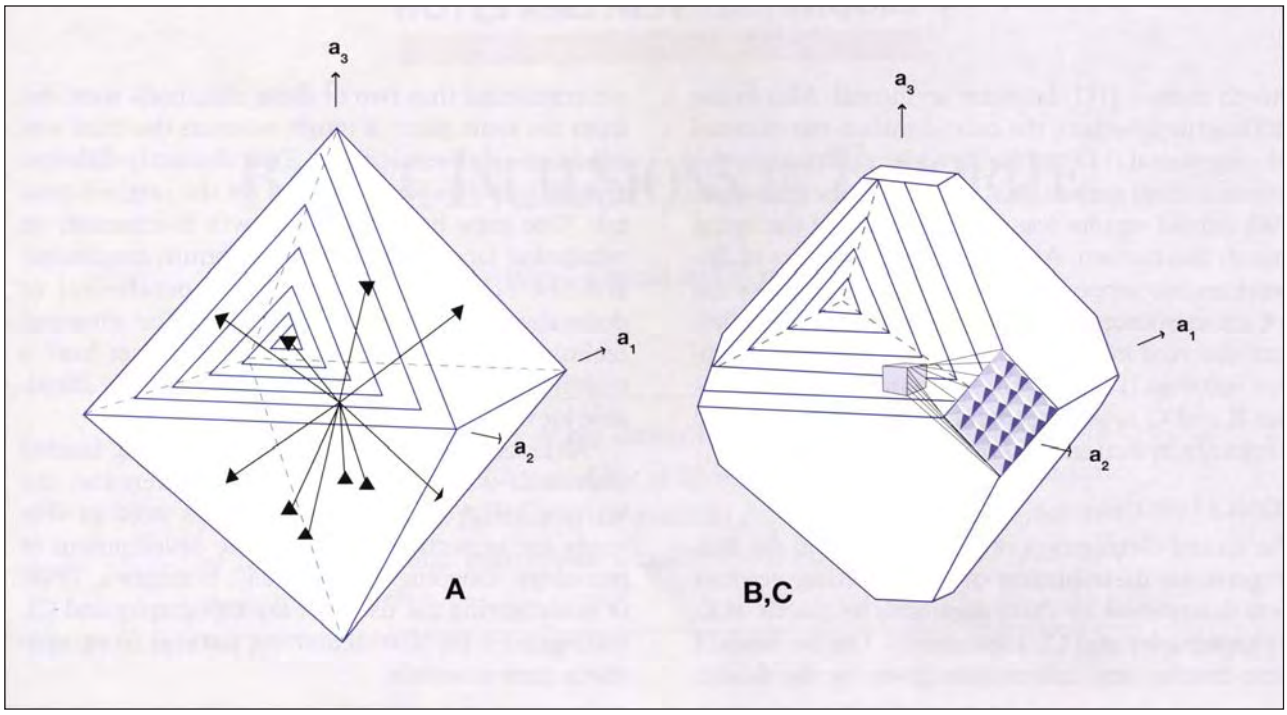

Figure 13. Samples B and C were cut from a crystal with a different morphology—and a more complicated growth history—than sample A. As shown on the left, sample A had a simple octahedral habit, bounded by {111} faces that grew by the spiral growth mechanism from the outcrop of dislocations. Several outcropping dislocations (the straight lines with triangular terminations) are shown, along with only one triangular growth spiral; each dislocation would be expected to produce a similar growth spiral during crystal growth. Samples B and C are assumed to have been cut from a dodecahedroid crystal with a rounded morphology that was due to post-growth dissolution of a crystal that originally consisted of stepped octahedral faces (equivalent to {110} faces) that were truncated by rough cuboid faces (right). The cuboid-shaped core acted as a seed for further growth of the surrounding portion. The straight lines that extend from the core to the cuboid face are dislocation bundles. Only part of the complicated growth history for this crystal is shown.

the spiral growth mechanism. The straight growth bands parallel to {111} are commonly encountered in single-crystal natural diamond, and they indicate a layer-by-layer (including spiral) growth mechanism on {111}, such that the octahedral habit was not modified throughout the growth history (Sunagawa, 1984b). It should be noted that even under such a steady growth condition, the nitrogen partitioning fluctuated, as shown by the alternating bright and dark CL zones. Such a zonation is attributed to local fluctuations in the growth rate.

Samples B and C showed a square-shaped core portion and much denser dislocation bundles in the <100> directions. Since most dislocations originate at the core boundary, there must have been an interruption of growth between the core and the surrounding material. A possible explanation is that the core formed under one set of growth conditions, and then was transported to a new growth environment where it acted as a seed for further diamond growth. This is the first observation of the presence of a seed crystal in natural diamond crystal growth.

The core took a cuboid form, bounded by rough cuboid surfaces (Sunagawa, 1984a), rather than an octahedral form. Further diamond growth on this seed transformed the morphology from cuboid to octahedral, or dodecahedral truncated by cuboid faces (i.e., that of a mixed habit). At the onset of growth over the cuboid seed, nitrogen was incorporated isotropically (i.e., equally over the seed surface, independent of crystallographic direction) into the crystal, giving rise to a bright CL band surrounding the seed surface. This also implies an abrupt change of growth parameters, which was followed by the appearance and development of {111} faces. In <110> growth sectors, {111} faces are flat; whereas in <100>

growth sectors, {111} faces are segmental. Also in the <100> growth sectors, the cuboid surface transformed into segmental {111} subfaces, while maintaining the general cuboid surface. It is likely that the growth of {100} cuboid sectors was not governed by the spiral growth mechanism. Although a large number of dislocations outcropped on the growing surface, they did not act as sources of spiral growth steps. The difference observed in interface roughness and growth process between {111} and {100} in sample A and samples B and C is in agreement with results reported previously by Sunagawa (1984b, 1995).

CONCLUSIONS

The spatial distribution of dislocations and the heterogeneous distribution of CL-emitting centers were determined for three diamonds by means of X-ray topography and CL tomography. On the basis of these results, and information given by the dealer, we concluded that two of these diamonds were cut from the same piece of rough, whereas the third was cut from a different crystal. Two distinctly different growth histories were revealed for the original crystals. One grew by the spiral growth mechanism on octahedral faces under near-equilibrium conditions, and the other showed growth of octahedral or dodecahedral forms on a cuboid seed. The advanced techniques employed require that the user have a technical background, but the equipment is affordable for most major gemological laboratories

Although the demand for fingerprinting faceted diamonds will depend on market preference, the writers believe that the techniques used in this study are important for the future development of gemology. Ongoing research (e.g., Sunagawa, 1998) is investigating the use of X-ray topography and CL tomography for distinguishing natural from synthetic gem materials.

REFERENCES

Clark C.D., Collins A.T., Woods G.S. (1992) Absorption and luminescence spectroscopy. In J.E. Field, Ed., *The Properties of Natural and Synthetic Diamond*, Academic Press, London, pp. 35–80.

Davies G. (1979) Cathodoluminescence. In J.E. Field, Ed., *The Properties of Diamond*, Academic Press, London, pp. 165–184.

Fersman A., Goldschmidt V. (1911) *Der Diamant*. Carl Winter's Universitätbuchhandlung, Heidelberg.

Frank F.C., Lang A.R. (1965) X-ray topography of diamond. In R. Berman, Ed., *Physical Properties of Diamond*, Clarendon Press, Oxford, pp. 69–115.

Lang A.R. (1978) Techniques and interpretation in X-ray topography. In S. Amelinckx, R. Gevers, and J. van Landuyt, Eds., *Diffraction and Imaging Techniques in Material Science*, Vol. II, North-Holland, Amsterdam, pp. 623–714.

Lang A.R. (1979) Internal structure. In J.E. Field, Ed., *The Properties of Diamond*, Academic Press, London, pp. 425–469.

Lang A.R., Moore M., Walmsley J.C. (1992) Diffraction and imaging studies of diamond. In J.E. Field, Ed., *The Properties of Natural and Synthetic Diamond*, Academic Press, London, pp. 215–258.

Ponahlo J. (1992) Cathodoluminescence (CL) and CL spectra of DeBeers experimental synthetic diamonds. *Journal of Gemmology*, Vol. 23, No. 1, pp. 3–18.

Scandale E. (1996) *X-ray Topographic Method for Minerals*. Lecture notes of Short Course on Crystal Growth in Earth Sciences, Santa Vittoria d'Alba, Italy, 14–19 April, pp. 361–374.

Schmetzer K. (1996) Growth method and growth-related properties of a new type of Russian hydrothermal synthetic emerald. *Gems & Gemology*, Vol. 32, No. 1, pp. 40–43.

Smith C.P. (1996) Introduction to analyzing internal growth structures: Identification of the negative *d* plane in natural ruby. *Gems & Gemology*, Vol. 32, No. 3, pp. 170–184.

Sunagawa I. (1984a) Growth of crystals in nature. In I. Sunagawa, Ed., *Materials Science of the Earth's Interior*, Terra, Tokyo and D. Reidel, Dordrecht, pp. 63–105.

Sunagawa I. (1984b) Morphology of natural and synthetic diamond crystals. In I. Sunagawa, Ed., *Materials Science of the Earth's Interior*, Terra, Tokyo and D. Reidel, Dordrecht, pp. 303–330.

Sunagawa I. (1988) Morphology of minerals. In I. Sunagawa, Ed., *Morphology of Crystals*, Part B, Terra, Tokyo and D. Reidel, Dordrecht, pp. 509–587.

Sunagawa I. (1995) The distinction of natural from synthetic diamonds. *Journal of Gemmology*, Vol. 24, No. 7, pp. 485–499.

Sunagawa I. (1998) Imperfections and inhomogeneities in single crystals as a basis to distinguish natural from synthetic gemstones. *Zeitschrift der Deutschen Gemmologischen Gesellschaft*, Vol. 47, No. 1, pp. 45–52.

Sunagawa I., Tsukamoto K., Yasuda T. (1984) Surface microtopographic and X-ray topographic study of octahedral crystals of natural diamonds from Siberia. In I. Sunagawa, Ed., *Materials Science of the Earth's Interior*, Terra, Tokyo and D. Reidel, Dordrecht, pp. 331–349.